SAND2011-3001C

MEASUREMENTS OF INSTABILITY AND TRANSITION IN HYPERSONIC BOUNDARY LAYERS

Katya M. Casper[1], **Steven P. Schneider**[2], **and Steven J. Beresh**[3]

[1]*Purdue University, 1375 Aviation Dr. West Lafayette, IN 47907, USA and Sandia National Labs, PO Box 5800, MS 0825, Albuquerque, NM 87185, USA, Email:kcasper@purdue.edu*
[2]*Purdue University, 1375 Aviation Dr. West Lafayette, IN 47907, USA, Email:steves@purdue.edu*
[3]*Sandia National Labs, PO Box 5800, MS 0825, Albuquerque, NM 87185, USA, Email:sjberes@sandia.gov*

ABSTRACT

Several studies on boundary-layer instability and transition have been conducted in the Boeing/AFOSR-Mach 6 Quiet Tunnel (BAM6QT) and the Sandia Hypersonic Wind Tunnels (HWT) at Mach 5 and 8. The first study looked at the effect of freestream noise on roughness-induced transition on a blunt cone. Temperature-sensitive paints were used to visualize the wake of an isolated roughness element at 0 deg angle of attack (AoA) in the BAM6QT. Transition was always delayed under quiet flow compared to noisy flow, even for an effective trip height. The second study measured transitional surface pressure fluctuations on a seven degree sharp cone in the HWT under noisy flow and in the BAM6QT under noisy and quiet flow. Fluctuations under laminar boundary layers reflected tunnel noise levels. Transition on the model only occurred under noisy flow, and fluctuations peaked during transition. Measurements of second-mode waves showed the waves started to grow under a laminar boundary layer, saturated, and then broke down near the peak in transitional pressure fluctuations. The third study looked at the development of wave packets and turbulent spots on the nozzle wall of the BAM6QT. A spark perturber was used to generate controlled disturbances. Measurements of the internal pressure structure of the disturbances were made.

Key words: Hypersonic Boundary-Layer Transition, Freestream Noise, Second-Mode Instability Waves, Turbulent Spots.

1. INTRODUCTION

Laminar-turbulent boundary-layer transition is important for hypersonic reentry vehicles since it affects parameters such as heat transfer, skin friction, and surface pressure fluctuations. Most ground tests studying boundary-layer transition are done in conventional hypersonic wind tunnels. These tunnels have turbulent boundary layers on the nozzle wall that radiate disturbances into the freestream. The noise level in these tunnels, defined as the root-mean-square (RMS) pitot pressure over the mean pitot pressure, is typically near 1% and sometimes as high as 2–5% [12]. These conventional tunnel noise levels are an order of magnitude higher than flight [2, 14]. Most research is still done in conventional tunnels making it important to understand the effect of noise on the results.

2. EXPERIMENTAL FACILITIES

2.1. Boeing/AFOSR Mach-6 Quiet Tunnel

The BAM6QT is one of two hypersonic quiet tunnels in the world. It can be operated as a conventional noisy tunnel or as a quiet tunnel. Quiet flow is obtained by opening bleeds slots at the throat to restart a laminar boundary layer. For noisy flow conditions, the bleeds are kept closed. The tunnel is a Ludwieg tube–a long tube with a converging-diverging nozzle on the end. The tunnel uses air as the test gas and operates with an initial total pressure P_0 of 34–2070 kPa and an initial total temperature T_0 of 430 K, giving a freestream unit Reynolds number (Re) range of 0.4–18.3×10^6/m. The current maximum quiet stagnation pressure is 1130 kPa. Noise levels vary from 2–4.5% under noisy flow conditions. Under quiet flow conditions, noise levels are less than 0.05% [16].

2.2. Sandia Hypersonic Wind Tunnel

The HWT is a blowdown-to-vacuum facility. Interchangeable nozzle and heater sections allow the tunnel to be run at Mach 5, 8, or 14. Mach 5 tests use air as the driver gas while Mach 8 and Mach 14 run with nitrogen. Tests were only conducted at Mach 5 and 8 for this study. HWT-5 has a P_0 range of 345–1380 kPa and a T_0 range of 330–890 K, giving a Re range of 3.3–26×10^6/m. HWT-8 has a P_0 range of 1720–6890 kPa, T_0 range of 500–890 K, and Re can be varied from 3.3–20×10^6/m.

3. EFFECT OF FREESTREAM NOISE ON ROUGHNESS-INDUCED TRANSITION FOR A SLENDER CONE

BAM6QT tests were done to show the effect of noise on transition downstream of an isolated roughness element. A parametric study of roughness-height effects on transition was also conducted.

The model was a 7 deg half-angle nylon cone with a 102-mm base diameter. The nylon portion of the cone stretches axially from 147 mm to 405 mm. The nosetip was stainless steel with a nose radius of 1.19 mm. The nylon section of the cone was painted with temperature-sensitive paint (TSP) which provides a surface temperature distribution that is used to visualize the roughness wake. The TSP is only qualitative for heat transfer at this time; the surface temperature is monotonic in the heat transfer. A single roughness element was placed on the model for each run as shown in Fig. 1. Roughness elements were 1.27 by 1.27-mm squares. Each trip was placed at an axial distance of 130 mm ($x/L = 0.32$) with a corner in line with the freestream. The trip height was varied between 0.36 and 0.71 mm during testing. Most tests were run starting at an initial stagnation temperature of 433 K and at the maximum quiet pressure of the tunnel. The freestream unit Reynolds number range of the pictures analyzed was between 8.7–10.0 $\times 10^6$ /m. Noise levels are near 2.5% at these conditions under noisy flow.

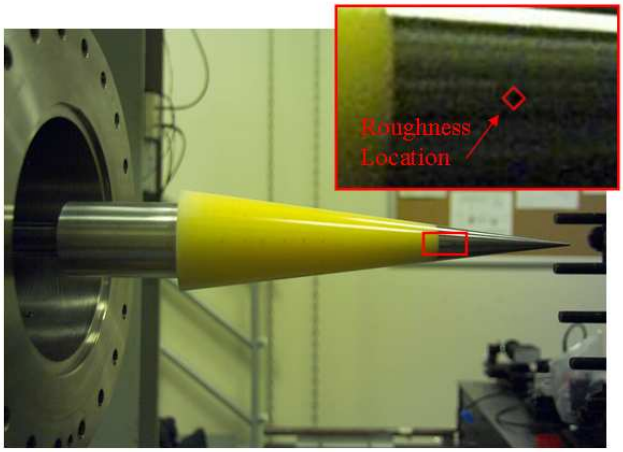

Figure 1. Model setup for testing in the BAM6QT

TSP images for the model under noisy and quiet flow for the minimum and maximum trip heights tested (0.36 and 0.71 mm, respectively) are shown in Fig. 2. These heights are 2.2 and 4.3 times the displacement thickness δ^* at the trip location. Results for intermediate trip heights can be found in [8, 9]. In most cases, the TSP shows two straight streaks in the wake of the roughness element. Downstream of the trip, the wake typically spreads and a turbulent wedge appears. Transition onset is inferred when a rise is seen in the centerline surface temperature. This is typically before the wake behind the trip starts to spread. Some of the trips are large enough to be considered effective. An effective trip is defined as one for which a further increase in height does not cause transition to move further forward.

Fig. 3 plots the roughness Reynolds number Re_k for each trip height against the transition onset location under both noisy and quiet flow. The smallest trip height corresponds to the smallest Re_k. Under noisy flow, the transition location behind the roughness element does not vary much, for the range of roughness heights tested. The smallest roughness height of 0.36 mm is not fully effective at 0° AoA. A further increase in trip height causes transition to move further forward. However, the 0.46-mm trip as well as the 0.53 and 0.71-mm trips cause transition at approximately the same location on the model. This indicates that the 0.46-mm trip was fully effective under noisy flow. Under quiet flow, the 0.36-mm high trip generates two hot streaks, but the flow remains laminar to the end of the cone. For the 0.46-mm high trip, transition begins just before the end of the model. The 0.53 and 0.71-mm high trips both cause transition downstream of the trip, but the transition location does not change significantly between these two trip heights. This indicates that the effective transition height for quiet flow conditions has been reached.

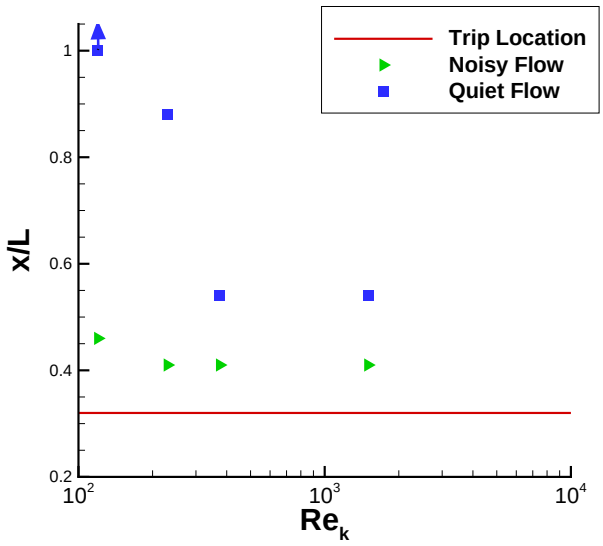

Figure 3. Effect of trip Reynolds number on transition location at 0 deg AoA.

A noticeable difference between noisy and quiet flow conditions can be seen. The same trip heights that cause transition on the model under noisy flow do not necessarily cause transition on the model in quiet flow. When transition does occur, it is delayed. For example, for a trip height of 0.46 mm, quiet flow delays transition by 6.3 times. It had been commonly assumed that tunnel noise would only affect transition location for less-than-effective trips [4, 15]. However, a significant delay in the transition location is still observed even with the largest trips, which are effective under quiet flow.

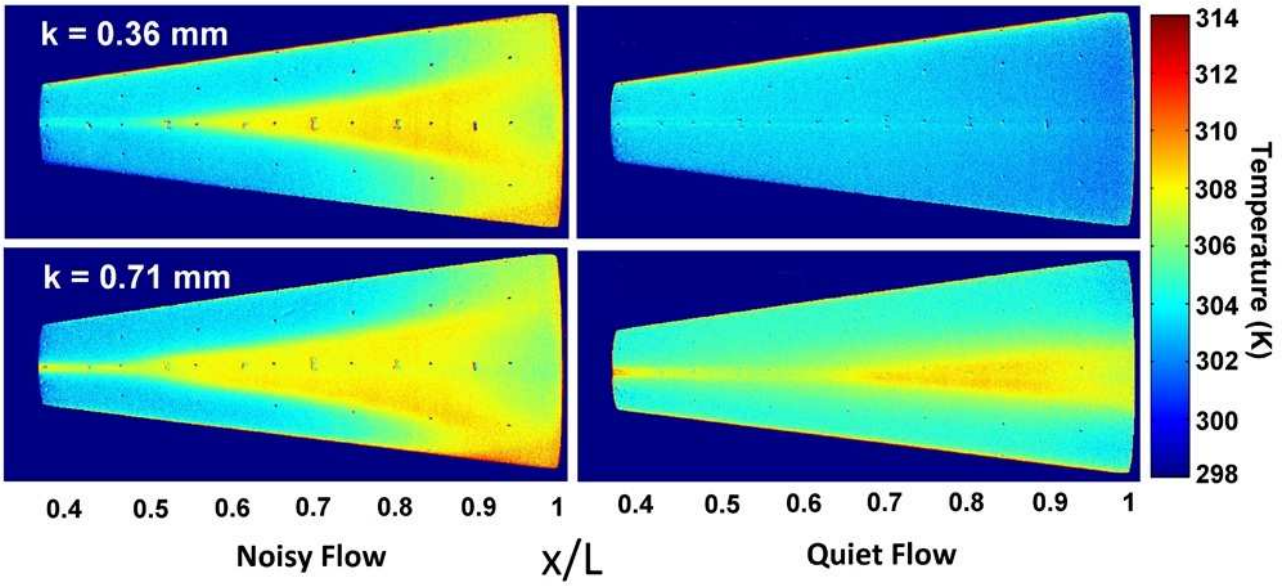

Figure 2. Effect of trip height under noisy and quiet flow. Trip location is at the left edge of each sub-figure ($x/L = 0.32$).

4. PRESSURE FLUCTUATIONS DURING BOUNDARY-LAYER TRANSITION

Hypersonic reentry vehicles are subjected to high levels of fluctuating pressures. These intense fluctuations can cause vibration of internal components and lead to structural fatigue. Current designs often use overly conservative estimates of the fluctuations that can lead to heavier vehicles and degraded flight performance. Some correlations exist for the magnitude of transitional and turbulent pressure fluctuations, but these were derived primarily using either incompressible data or conventional (noisy flow) hypersonic wind-tunnel tests [13]. Too little physical understanding of the generation of transitional pressure fluctuations has resulted from such modeling efforts. In order to improve prediction of hypersonic pressure fluctuations, surface pressure fluctuations were measured on a 7 deg sharp cone at 0 AoA. Experiments under noisy flow were conducted in the HWT at Mach 5 and 8 and in the BAM6QT at Mach 6. Measurements under quiet flow were also conducted in the BAM6QT.

The cone model was designed with two rows of instrumentation, 120° apart. Sensors can be placed in either row at 8 axial locations from the nosetip. Kulite XCQ-062-15A and Mic-062 sensors were used to measure pressure fluctuations between 0 and 50 kHz. The XCQ-062 sensors have a resonant frequency between 250–300 kHz while the Mic-062 sensors have a lower resonant frequency near 125 kHz. For these tests, only A-screen sensors were used. The A-screen has a large central hole. This screen offers only a small amount of diaphragm protection, but the sensor has a flatter frequency response. PCB132 sensors were used to measure higher frequencies between 11 kHz and 1 MHz; The resonant frequency of the sensors is above 1 MHz, but the sensor output is high-pass filtered at 11 kHz, per the manufacturer's specifications. Because the resonant frequency of the PCB132's is high, the sensors can measure high-frequency instabilities leading to transition in hypersonic flows [3, 5, 10, 11]. The sensors are useful indicators of transition on the model.

Pressure fluctuations between 0 and 50 kHz were measured along the cone surface in each tunnel. Fig. 4 shows a typical result in HWT-5 where the fluctuations are normalized by the nozzle wall shear stress τ_w. Using τ_w to normalize the fluctuations collapsed the laminar fluctuations much better than the edge pressure or edge dynamic pressure. Laminar fluctuations are seen in the first three sensors below $Re = 12.7 \times 10^6$/m. Downstream, a peak is seen in the pressure fluctuations during transition, and the peak moves further forward with increasing Re. Similar results were obtained in the BAM6QT and in HWT-8 [5, 6].

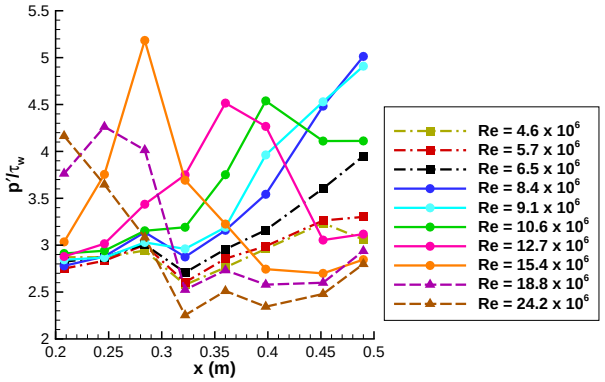

Figure 4. Surface pressure fluctuations (HWT-5)

High frequency measurements with the PCB132 sensors

allow resolution of the instabilities leading to transition on the cone. Fig. 5(a) shows a typical power spectral density (PSD) when transition occurs over the middle portion of the cone at Mach 8. The first sensor is under fully laminar flow. A large-amplitude second-mode wave at 320 kHz as well as a harmonic at 640 kHz can be seen. The second sensor at x = 0.360 m is in the middle of the peak fluctuations seen by the Kulite sensors (Fig. 5(b)). In this case, the second-mode waves near 230 kHz have started to break down but are still visible. Higher frequency broadband components are seen throughout the spectrum. The third sensor at x = 0.490 m corresponds to turbulent flow as indicated by the Kulite fluctuations. The second-mode waves are no longer visible on the cone, and there are now broadband frequency components.

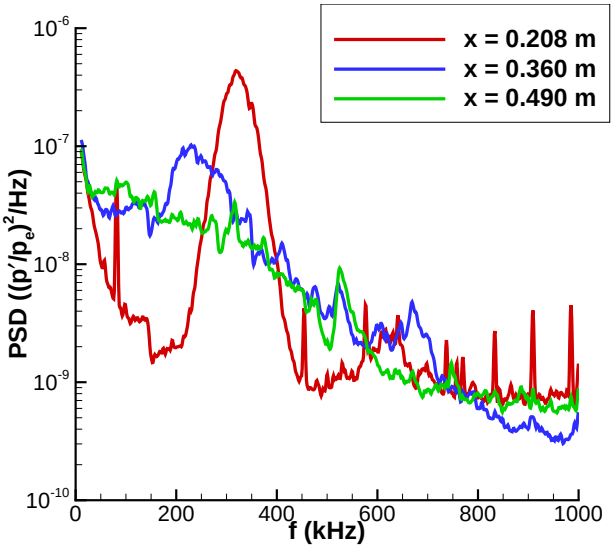

(a)

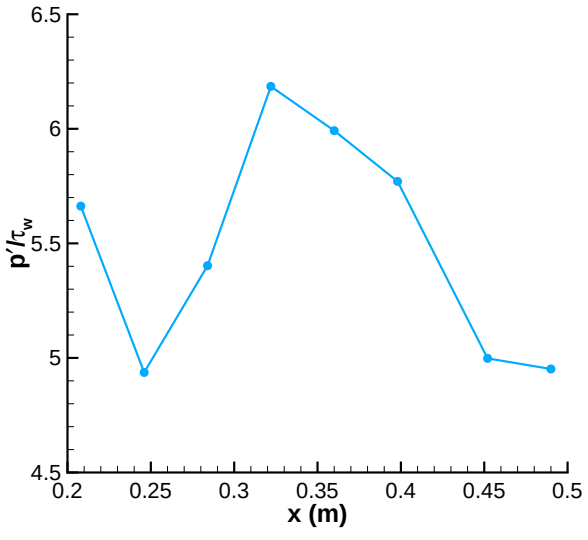

(b)

Figure 5. Comparison of PCB132 spectra and transition defined by Kulites (HWT-8, $Re = 9.5 \times 10^6$/m)

These instability measurements can be compared to linear stability theory computations. Computations using the STABL software suite are described in detail in [1]. Fig. 6 shows a comparison between computations and second-mode wave measurements in HWT-8 at $Re = 5.0 \times 10^6$/m. At x = 0.208 m, the computed second-mode frequency peak is within 5% of the measured peak. Since higher harmonics are not present, it is believed that this is still the linear growth stage. A second harmonic can be seen in the normalized pressure fluctuation at x = 0.360 m, but the computations still accurately predict the most amplified second-mode frequency to within 4%. By x = 0.490 m, transition onset has been observed in the experiment. Higher harmonics are present in the signal and there is a more broadband frequency spectrum. However, the computed and measured second-mode peak frequency still compare well with a 5% difference.

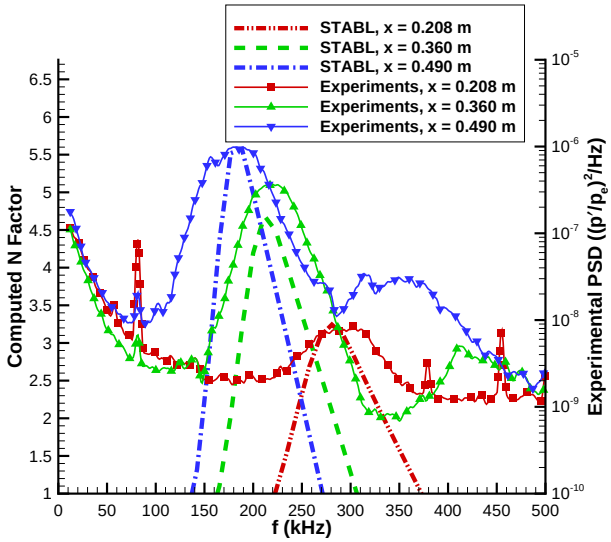

Figure 6. Comparison of experimentally measured and computed second-mode waves (HWT-8)

Because the BAM6QT can be run with either noisy or quiet flow, the tunnel provides a unique environment to show noise effects on the measured pressure fluctuations. The cone was run under quiet-flow conditions that matched the noisy-flow Re. In all quiet-flow cases, the flow remained laminar over the entire cone, even when transition occurred well forward on the model under noisy flow. The pressure fluctuations are almost an order of magnitude lower under quiet flow. Tunnel noise also has an effect on the growth of instability waves. Fig. 7 shows a comparison of waves measured under quiet flow compared to noisy-flow results. Second-mode waves can be seen at 220 and 235 kHz under quiet flow. The RMS amplitude of the quiet-flow waves is approximately 0.34%, more than an order of magnitude lower than under noisy flow. Under noisy flow, the waves are centered at 330 and 350 kHz and the RMS amplitude of the waves is 5.0%. However, these waves cannot be directly compared. Under quiet flow, the waves are only seen at the last sensor location (x = 0.490 m). The noisy-flow waves appear at the first sensor location (x = 0.208 m) and have broken down by the end of the cone.

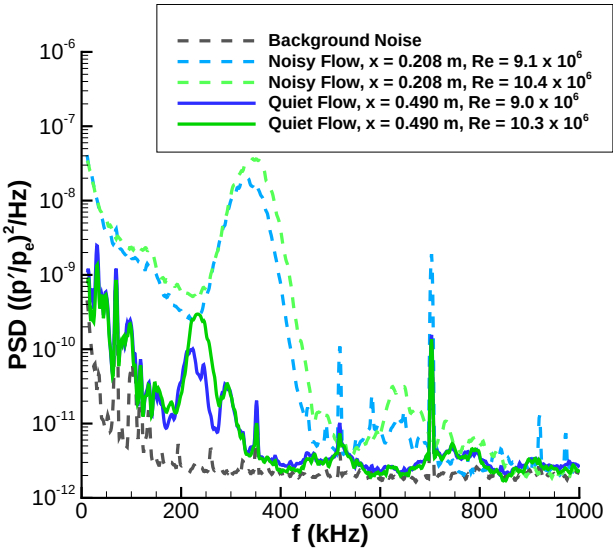

Figure 7. Second-mode waves under noisy and quiet flow (BAM6QT)

These results confirm that pressure fluctuations do peak during boundary-layer transition. Tunnel noise affects not only transition location on the cone, but also measurements of pressure fluctuations under a laminar boundary layer. In addition, the growth of the second-mode waves is affected by tunnel noise. More in-depth analysis of these results is found in [1, 5, 6].

5. INSTABILITY WAVES AND TURBULENT SPOTS ON THE BAM6QT NOZZLE WALL

Measurements on the 7 deg cone showed a transitional pressure fluctuation peak, but turbulent spots could not be clearly identified in the time traces [5]. This was likely due to the frequency-response limitations of the pressure transducers. The boundary layer on the cone is only a few mm thick and transition occurs over a short length. The turbulent spots are small (on the order of a cm) and the sensors did not have the appropriate frequency response or spatial resolution to detect individual spots. In order to study turbulent spots within the instrumentation limits, measurements were made in the thick boundary layer on the nozzle wall of the BAM6QT. In order to study controlled disturbances, a spark perturber was used to create large impulses.

A schematic of the experimental setup is shown in Fig. 8. Nozzle wall pressure fluctuations were measured with four XCQ-062-15A sensors at z = 2.201, 2.302, 2.378, and 2.480 m, where z is the axial tunnel coordinate measured from the throat (Fig. 8). A spark perturber was located at z = 1.924 m, upstream of this plug in another insert on the top wall of the tunnel. Additional Kulites were located at z = 2.628, 2.679, 2.730, 2.781, and 2.831 m on the top wall of an insert downstream of the nozzle exit. These sensors locations are marked on the axis in Fig. 8.

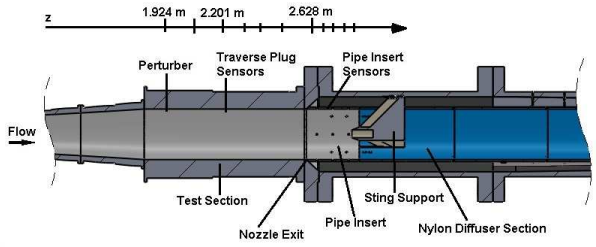

Figure 8. Schematic of experimental setup in BAM6QT. Perturber and sensor locations are marked on the z axis.

Because the spark perturbations are generated at 200 Hz, multiple disturbances can be averaged. Ensemble-averaged pressure traces are shown for 50 disturbances. These disturbances were chosen from a 0.5-s interval, after the perturber had been running for a few tenths of a second. More repeatable results are obtained after the perturber has warmed up. Also, even though Re drops within this 0.5-s interval, the change is less than 1% and no noticeable affects are seen on the results. Any disturbances that were contaminated by naturally-occurring turbulent spots or smaller disturbances were not used in the averages. An ensemble-averaged PSD was also computed by averaging together fast-Fourier transforms (FFT's) from each of the 50 pressure traces and normalizing to obtain the PSD. This ensemble-averaged power-spectral density is not the same as taking a PSD of the ensemble-averaged pressure traces. This difference is most apparent when wave packets began to break down. Even though the packets show good repeatability while growing, their breakdown varies from packet-to-packet, and the pressure fluctuations are no longer in phase. As a result, the ensemble-averaged pressure traces smooth out the turbulent fluctuations seen during breakdown. Since phase information is not contained in the FFT, ensemble averaging FFT's together does not remove the large fluctuations during breakdown but instead creates an average representation of the frequency content of the individual samples.

The resulting ensemble-averaged disturbances created by the spark near the highest quiet Re are shown in Fig. 9. Results for other freestream conditions can be found in [7]. The fluctuating component of the pressure is shown normalized by the freestream pressure. Traces are vertically offset from each other proportional to z to show the growth of the disturbances. A wave packet is initially generated by the spark perturbation. The packet grows downstream, and its peak frequency decreases from 50 to 43 kHz as the boundary layer thickens. These frequencies are in good agreement with instability computations. Further downstream, the wave packet becomes nonlinear and breaks down into a turbulent spot by z = 2.679 m. Breakdown occurs first in the middle of the packet, with second-mode waves still visible on either side of the breakdown. As the spot grows, the turbulent region lengthens. However, there is still evidence of the second-mode waves on either side of the spot. There is no sudden transition from instability waves to turbulent fluc-

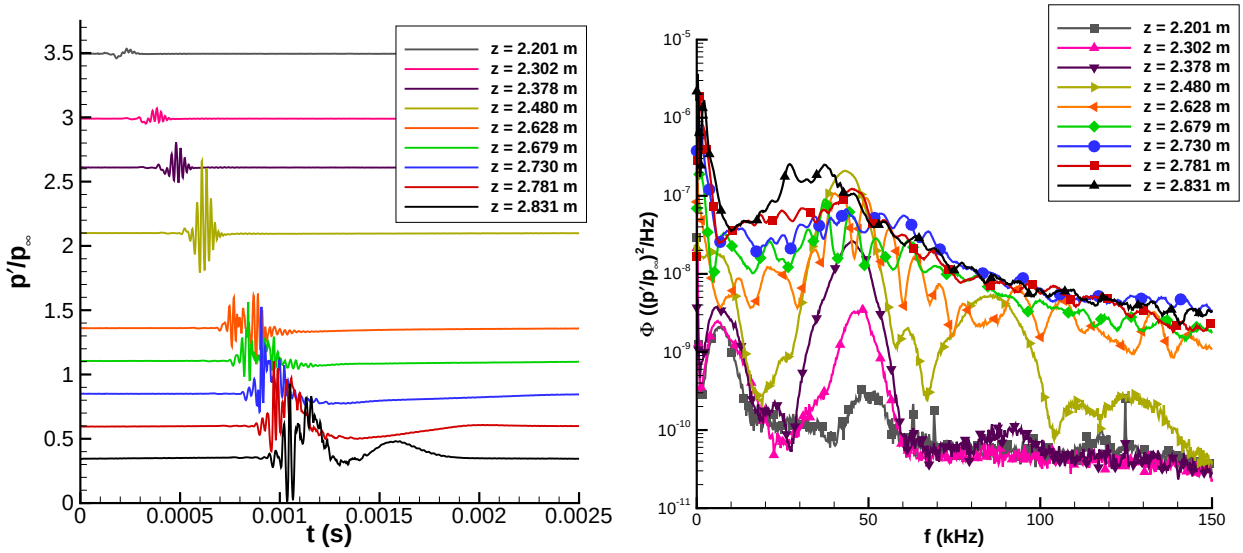

(a) (b)

Figure 9. Ensemble-averaged disturbances from spark perturbations, P_0 = 1084 kPa, T_0 = 423.8 K, $Re = 10.8 \times 10^6/m$; (a) Pressure traces, each trace is vertically offset proportional to z; (b) Power spectral density.

tuations. Instead there is a gradual growth and breakdown of the waves into turbulent spots. As a result, there is a long region where instability waves are seen while turbulent fluctuations are observed growing within the spot. As the spot grows, the fluctuations at the beginning of the spot are still visible, but the second-mode waves behind the spot become more out of phase and tend to average out. These measurements allow computations of both wave-packets and turbulent spot convection velocities. The amplitude of the waves at breakdown can also be obtained from these measurements.

ACKNOWLEDGMENTS

John Phillips designed and built the spark perturber. Erick Swanson provided advice and assistance throughout the roughness-induced transition studies. Peter Gilbert created the CAD model used to generate Fig. 1. Funding was provided in part by an NDSEG Fellowship, the NSF GRFP, Sandia National Laboratories, and AFOSR.

REFERENCES

[1] Alba, C., Casper, K., & Schneider, S. 2010, Comparison of Experimentally Measured and Computed Second-Mode Disturbances in Hypersonic Boundary Layers, AIAA Paper 2010-897

[2] Beckwith, I. E. & Miller III, C. G. 1991, Annual Review of Fluid Mechanics, 22, 419

[3] Berridge, D. C. 2010, Master's thesis, Purdue University School of Aeronautics & Astronautics

[4] Berry, S. A. & Horvath, T. J. 2008, Journal of Spacecraft and Rockets, 45, 216

[5] Casper, K. M. 2009, Master's thesis, Purdue University School of Aeronautics & Astronautics

[6] Casper, K. M., Beresh, S. J., Henfling, J. F., et al. 2009, Hypersonic Wind-Tunnel Measurements of Boundary-Layer Pressure Fluctuations, AIAA Paper 2009-4054

[7] Casper, K. M., Beresh, S. J., & Schneider, S. P. 2011, Pressure Fluctuations Beneath Turbulent Spots and Instability Wave Packets in a Hypersonic Boundary Layer, AIAA Paper 2011-372

[8] Casper, K. M., Johnson, H. B., & Schneider, S. P. 2011, Journal of Spacecraft and Rockets, accepted for publication

[9] Casper, K. M., Wheaton, B. M., Johnson, H. B., & Schneider, S. P. 2008, Effect of Freestream Noise on Roughness-Induced Transition at Mach 6, AIAA Paper 2008-4291

[10] Estorf, M., Radespiel, R., Schneider, S. P., Johnson, H., & Hein, S. 2008, Surface-Pressure Measurements of Second-Mode Instability in Quiet Hypersonic Flow, AIAA Paper 2008-1153

[11] Fujii, K. 2006, Journal of Spacecraft and Rockets, 43, 731

[12] Laderman, A. J. 1977, AIAA Journal, 15, 605

[13] Laganelli, A. L., Martellucci, A., & Shaw, L. L. 1983, AIAA Journal, 21, 495

[14] Schneider, S. P. 2001, Journal of Spacecraft and Rockets, 38, 323

[15] Schneider, S. P. 2008, Journal of Spacecraft and Rockets, 45, 193

[16] Steen, L. E. 2010, Master's thesis, Purdue University School of Aeronautics & Astronautics